Acta Crystallographica Section C
Crystal Structure Communications
ISSN 0108-2701

Sodium magnesium sulfate decahydrate, $Na_2Mg(SO_4)_2 \cdot 10H_2O$, a new sulfate salt

Evelyne M. S. Leduc,[a] Ronald C. Peterson[a]* and Ruiyao Wang[b]

[a]Department of Geological Sciences and Geological Engineering, Queen's University, Kingston, Ontario, Canada K7L 3N6, and [b]Department of Chemistry, Queen's University, Kingston, Ontario, Canada K7L 3N6
Correspondence e-mail: peterson@geol.queensu.ca

Received 8 June 2009
Accepted 21 July 2009
Online 24 October 2009

The structure of synthetic disodium magnesium disulfate decahydrate at 180 K consists of alternating layers of water-coordinated $[Mg(H_2O)_6]^{2+}$ octahedra and $[Na_2(SO_4)_2(H_2O)_4]^{2-}$ sheets, parallel to [100]. The $[Mg(H_2O)_6]^{2+}$ octahedra are joined to one another by a single hydrogen bond, the other hydrogen bonds being involved in inter-layer linkage. The Mg^{2+} cation occupies a crystallographic inversion centre. The sodium–sulfate sheets consist of chains of water-sharing $[Na(H_2O)_6]^+$ octahedra along *b*, which are then connected by sulfate tetrahedra through corner-sharing. The associated hydrogen bonds are the result of water–sulfate interactions within the sheets themselves. This is believed to be the first structure of a mixed monovalent/divalent cation sulfate decahydrate salt.

Comment

Sodium magnesium sulfate decahydrate belongs to a group of sulfate salts having the general formula $Na_2Mg(SO_4)_2 \cdot nH_2O$. Konyaite ($n$ = 5) and blödite (n = 4) are two known mineral phases of this type, and are most commonly found as salt efflorescences associated with marine and lacustrine sediments. Such environments can be found in areas like the Great Konya Basin, Turkey (van Doesburg *et al.*, 1982), the northern Great Plains of North Dakota (Keller *et al.*, 1986*a*) and western Canada (Last & Ginn, 2005), as well as in the Carrizo Plain, California (Eghbal *et al.*, 1989). Na–Mg sulfate decahydrate is suspected to occur in similar environments, as it readily dehydrates to konyaite. These phases are sensitive to changes in temperature and relative humidity, and precipitate chiefly through evaporative concentration of saline solutions (Keller *et al.*, 1986*b*).

The behavior and stability of $Na_2Mg(SO_4)_2 \cdot nH_2O$ phases and other phases of the Na_2O–MgO–SO_4–H_2O system are related, at least partially, to the arrangement and importance of the hydrogen bonds in their structure. Consequently, numerous studies have focused on solving their crystal structures, and individual phases are relatively well described, for example, blödite [$Na_2Mg(SO_4)_2 \cdot 4H_2O$; Rumanova, 1958; Hawthorne, 1985], epsomite ($MgSO_4 \cdot 7H_2O$; Baur, 1964), hexahydrite ($MgSO_4 \cdot 6H_2O$; Zalkin *et al.*, 1964), vanthoffite [$Na_6Mg(SO_4)_4$; Fischer & Hellner, 1964], löweite [$Na_{12}Mg_7(SO_4)_{13} \cdot 15H_2O$; Fang & Robinson, 1970; Nord, 1973], thenardite (Na_2SO_4; Hawthorne & Ferguson, 1975), mirabilite ($Na_2SO_4 \cdot 10H_2O$; Levy & Lisensky, 1978) and konyaite [$Na_2Mg(SO_4)_2 \cdot 5H_2O$; Leduc *et al.*, 2009].

The interactions and stability relationships between these phases, however, are poorly understood. Although phase relationships for the system have been partially mapped out (Archibald & Gale, 1924; Blasdale & Robson, 1928; Keller *et al.*, 1986*a*), and these studies have been tied to field studies of saline soils of the Great Konya Basin by Driessen & Schoorl (1973), the existence of metastable phases, or the status of some of these minerals as being metastable, has been debated. D'Ans (1933) suggested, for instance, that the blödite field of stability could include a metastable phase, which was later found by Friedel (1976) to have the formula $Na_2Mg(SO_4)_2 \cdot 5H_2O$. Konyaite was, however, not fully recognised until 1982 (van Doesburg *et al.*, 1982). Timpson *et al.* (1986) later questioned its status as a metastable phase, and its structure was only described much later (Leduc *et al.*, 2009). This study introduces another phase to the system.

These sulfates are typically labile and constitute important components of saline soils, playing a role in desertification, soil contamination, and surface and ground water salinization (Shayan & Lancucki, 1984; Timpson *et al.*, 1986; Keller *et al.*, 1986*a*; Whittig *et al.*, 1982; Last, 2002). They are also often associated with reactions involving mine waste (Zielinski *et al.*, 2001) and commonly cause damage to concrete structures (Gao *et al.*, 2007), both areas of ongoing concern. Furthermore, they occur in terrestrial environments that are used as analogs to what the Martian surface and subsurface environments are believed to be like (King *et al.*, 2004). The study of these terrestrial analogs has already led to the discovery of a new mineral that is predicted to occur on Mars (Peterson & Wang, 2006; Peterson *et al.*, 2007), and numerous other sulfate phases have been identified on its surface (Christensen *et al.*, 2004; Squyres *et al.*, 2004). The large saline oceans and icy crust of the Jovian moon Europa are also believed to include some phases belonging to the Na_2O–MgO–SO_4–H_2O system (Dalton, 2007; Dalton *et al.*, 2005; Kargel *et al.*, 2000). A greater understanding of the behavior of this system on Earth may therefore be applicable to these other environments.

The decahydrate structure contains two cation sites filled by Mg, in a slightly distorted octahedral arrangement, and Na, in a significantly more distorted octahedral coordination (Fig. 1 and Table 1). Of the five symmetrically unique water molecules, three coordinate exclusively with the Mg cations (O3*W*, O4*W* and O5*W*), while the other two (O1*W* and O2*W*) coordinate the Na cations only.

The Mg octahedra interact with each other by O4*W*—H4*A*$\cdots$O3*W*^{v} [symmetry code: (v) $x, -y + \frac{3}{2}, z - \frac{1}{2}$] hydrogen

doi:10.1107/S0108270109028881

bonds alone, whereas the Na polyhedra share edges with one another, forming chains along *b*. These edges are defined by the sharing of O1*W* and O2*W* atoms between Na atoms. The remaining bonds are satisfied by corner-sharing between the Na octahedra and sulfate tetrahedra. This corner-sharing, together with water–sulfate O—H···O hydrogen bonds involving atoms H1 and H2, links the Na octahedra chains to form sheets perpendicular to *a*. These sheets are separated by layers of weakly interacting Mg octahedra (Fig. 2). Several H atoms on the Mg-coordinated water molecules are involved in bonding the $[Mg(H_2O)_6]^{2+}$ layers to the sulfate O atoms of the $[Na_2(SO_4)_2(H_2O)_4]^{2-}$ layers (Table 2). A bond valence summation was calculated for the structure, following the method of Brown (1981) and using the curve provided by Ferraris & Ivaldi (1988) for long hydrogen-bond contributions. The results confirm that the proposed structure solution is reasonable.

The decahydrate structure, while distinct, bears certain similarities to that of both konyaite ($n = 5$) and blödite ($n = 4$). These features suggest a trend in the way the initial tetrahydrate structure must be modified to accommodate five and then ten water molecules. All three compounds are monoclinic, with a layered structure where hydrogen bonds are important.

The layers of the blödite structure are described as open sheets composed of water-coordinated Mg–sulfate clusters, $[Mg(SO_4)_2(H_2O)_4]^{2-}$, linked by pairs of edge-sharing Na octahedra and hydrogen bonds (Hawthorne, 1985). All sheets are identical, and are tied to one another by corner-sharing between sulfate tetrahedra and both the Mg and the Na octahedra. Hydrogen bonds are also involved in inter-sheet bonding. The Mg octahedra form an integral part of each sheet.

The konyaite structural layers have a much denser arrangement, where all polyhedra share at least one edge with a neighbor but can share up to three (Leduc *et al.*, 2009). Corner-sharing is secondary and only involved in the formation of chains, which are then bonded together through further edge-sharing to form layers. Inter-layer linkage involves hydrogen bonds exclusively. Two symmetrically independent Na sites are present; an octahedral and an eight-coordinated site are required to accommodate the presence of the 'fifth' water molecule that now coordinates the Mg atom. The Na sites still occur in edge-sharing pairs, but the eight-coordinated sites are responsible for the formation of the polyhedral chains, whereas the octahedral sites provide linkage between the chains, effectively creating the layers. The Mg octahedra are located on the outside of each chain and provide the hydrogen bonds holding the layers to one another.

The decahydrate structure follows the same trend, as the Mg atoms are now coordinated by six water molecules, to accommodate the 'extra' water molecules. This limits corner- and edge-sharing for the Mg octahedra and, as a result, they now form a separate layer, whose structure relies entirely on hydrogen bonding. It seems that the structures tend to segregate Na and Mg polyhedra as water content increases. The Na atoms must now coordinate the remaining four water molecules, which again allows for a symmetrically unique Na octahedral site, as in blödite. The Na octahedra no longer occur in pairs but retain the chain element through edge-sharing. As in konyaite, the chains are assembled together to form the layers, but corner-sharing is involved as in blödite, as opposed to the very compact nature of the konyaite layers which requires edge-sharing to bind chains together. Finally, only hydrogen bonds provide inter-layer linkage in the decahydrate, as they do in konyaite, and account for the tabular habit and cleavage of both compounds. The blödite layers, on

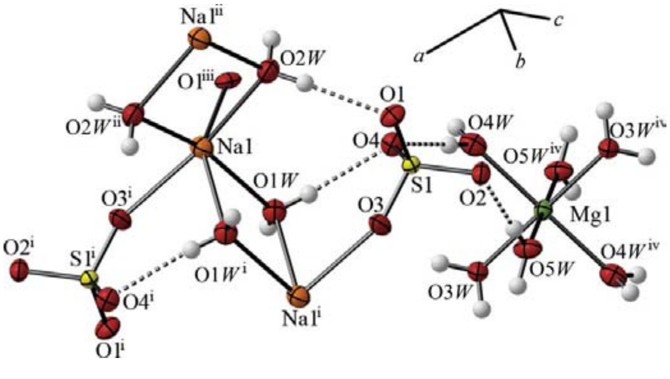

Figure 1
The coordination environment of the decahydrate asymmetric unit, showing displacement ellipsoids for non-H atoms at the 70% probability level. H atoms are depicted as spheres of arbitrary radii, and their labels have been omitted for clarity. Dashed lines represent hydrogen bonds. [Symmetry codes: (i) $-x + 2, -y + 1, -z + 1$; (ii) $-x + 2, -y, -z + 1$; (iii) $x, -y + \frac{1}{2}, z - \frac{1}{2}$; (iv) $-x + 1, -y + 2, -z + 1$.]

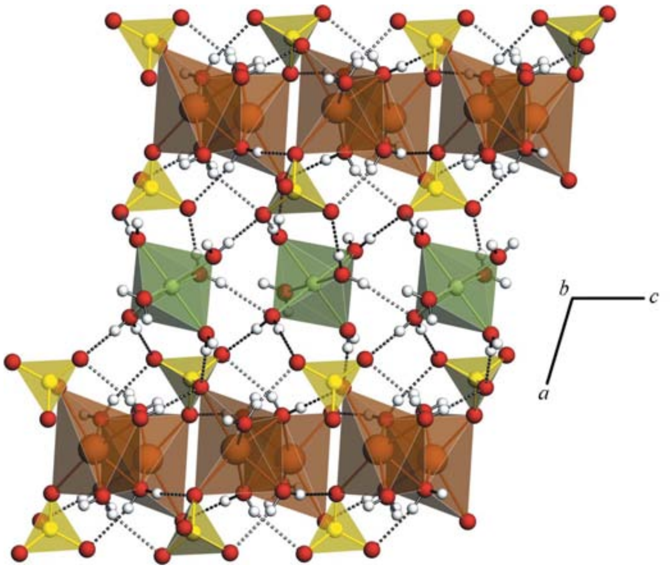

Figure 2
The decahydrate structure, as viewed down the *b* axis. This geometry accounts for the [100] cleavage, as layers are only linked to one another by hydrogen bonds. [In the electronic version of the paper, Mg octahedra (slightly distorted) are green, Na octahedra (distorted) are orange, sulfate tetrahedra are yellow, O atoms are red and H atoms are white.]

the other hand, involve both hydrogen bonding and corner-sharing in sheet-to-sheet linkage.

Several other types of structures exist for compounds having the general formula $M_2M'(SO_4)_2{\cdot}nH_2O$, where M is a monovalent cation (typically Na, NH_4 or K, but may include Rb, Cs, *etc.*), M' is a divalent cation (usually Mg, Ca or a transition metal) and n denotes the hydration state. Examples include monohydrates, dihydrates and hexahydrates. No decahydrate analogues (n = 10) have been reported in the literature.

The hexahydrate type of structure can accommodate a variety of cations, the most common of which are NH_4^+ and K^+, and Mg^{2+}, Ca^{2+} or a first row divalent transition metal. Although the arrangement of the structure slightly varies depending on composition, the overall connectivity is comparable. Therefore, picromerite [$K_2Mg(SO_4)_2{\cdot}6H_2O$; Kannan & Viswamitra, 1965] was selected for comparison, as it is an Mg phase. The structure is composed of undulating layers, where chains of corner-sharing distorted K-centered octahedra are linked by water-coordinated Mg octahedra and sulfate tetrahedra through corner-sharing as well as hydrogen bonding. Aside from the presence of a chain arrangement, this type of structure is more similar to that of blödite than to the decahydrate, as the sheets are all identical, contain both metal sites, and rely on corner-sharing and hydrogen bonding for connectivity.

The decahydrate structure, therefore, includes features present in the structures of other phases having the same general formula. However, the difference in composition of its layers, the chain arrangement present in the sodium sulfate layer and the importance of hydrogen bonding to its overall connectivity distinguish it from the other $M_2M'(SO_4)_2{\cdot}nH_2O$ phases.

Experimental

The crystal used in this study was synthesized according to the method described by van Doesburg *et al.* (1982). Solutions with a 1:1 molar ratio of reagent-grade $MgSO_4$ and Na_2SO_4 were prepared by dissolving magnesium sulfate (20 g) and sodium sulfate (23.6 g) in distilled water (160 ml). These solutions were evaporated between 297 and 301 K, and 51 to 64% relative humidity, in large Petri dishes with perforated covers. Concentrations sufficient for precipitation were typically reached in 72–96 h. The synthesized crystals have a rhombic habit and measure between <1 and 5 mm typically, although crystals as large as 2 cm were obtained with slower evaporation rates. The rhombs are soft, colorless and transparent, and exhibit a [100] cleavage. A single-crystal fragment of the synthetic material was selected, immersed in mineral oil to prevent dehydration and inserted in a 0.3 mm glass capillary at 180 K, which was then mounted for single-crystal X-ray diffraction.

Crystal data

$Na_2Mg(SO_4)_2{\cdot}10H_2O$
M_r = 442.57
Monoclinic, $P2_1/c$
a = 12.4950 (13) Å
b = 6.4978 (7) Å
c = 9.9943 (11) Å
β = 106.362 (1)°
V = 778.57 (14) Å^3
Z = 2
Mo $K\alpha$ radiation
μ = 0.53 mm^{-1}
T = 180 K
0.30 × 0.24 × 0.08 mm

Table 1
Selected geometric parameters (Å, °).

Mg1—O4*W*	2.0405 (14)	Na1—O2*W*	2.4495 (17)
Mg1—O5*W*	2.0466 (14)	Na1—O2*W*$^{\rm ii}$	2.4765 (17)
Mg1—O3*W*	2.1089 (14)	Na1—O1$^{\rm iii}$	2.5182 (15)
Na1—O1*W*$^{\rm i}$	2.4018 (16)	Na1—O3$^{\rm i}$	2.3822 (15)
Na1—O1*W*	2.4139 (17)		
O4*W*$^{\rm iv}$—Mg1—O5*W*$^{\rm iv}$	92.48 (6)	O1*W*$^{\rm i}$—Na1—O1*W*	77.44 (6)
O4*W*$^{\rm iv}$—Mg1—O3*W*$^{\rm iv}$	90.11 (6)	O1*W*—Na1—O2*W*	105.43 (6)
O5*W*$^{\rm iv}$—Mg1—O3*W*$^{\rm iv}$	87.38 (6)	O1*W*—Na1—O1$^{\rm iii}$	75.50 (5)
O3$^{\rm i}$—Na1—O1*W*	87.58 (6)	O2*W*—Na1—O1$^{\rm iii}$	84.11 (5)
O3$^{\rm i}$—Na1—O2*W*	164.66 (6)	O2*W*$^{\rm ii}$—Na1—O2*W*	77.18 (6)

Symmetry codes: (i) $-x+2, -y+1, -z+1$; (ii) $-x+2, -y, -z+1$; (iii) $x, -y+\frac{1}{2}, z-\frac{1}{2}$; (iv) $-x+1, -y+2, -z+1$.

Table 2
Hydrogen-bond geometry (Å, °).

D—H⋯A	D—H	H⋯A	D⋯A	D—H⋯A
O1*W*—H1*A*⋯O4	0.811 (15)	2.111 (17)	2.9008 (19)	164 (3)
O1*W*—H1*B*⋯O3$^{\rm v}$	0.821 (15)	1.993 (15)	2.804 (2)	169 (2)
O2*W*—H2*A*⋯O1	0.819 (15)	1.986 (15)	2.804 (2)	175 (3)
O2*W*—H2*B*⋯O2$^{\rm iii}$	0.816 (15)	2.324 (19)	3.082 (2)	155 (3)
O3*W*—H3*A*⋯O2$^{\rm vi}$	0.820 (15)	1.914 (15)	2.731 (2)	174 (3)
O3*W*—H3*B*⋯O4$^{\rm vii}$	0.809 (15)	2.013 (15)	2.822 (2)	177 (3)
O4*W*—H4*A*⋯O3*W*$^{\rm v}$	0.814 (14)	2.177 (15)	2.979 (2)	168 (2)
O4*W*—H4*B*⋯O4	0.814 (14)	1.939 (15)	2.7529 (19)	178 (3)
O5*W*—H5*A*⋯O2	0.821 (15)	1.915 (16)	2.731 (2)	173 (3)
O5*W*—H5*B*⋯O1$^{\rm viii}$	0.820 (15)	1.940 (15)	2.756 (2)	173 (3)

Symmetry codes: (iii) $x, -y+\frac{1}{2}, z-\frac{1}{2}$; (v) $x, -y+\frac{3}{2}, z-\frac{1}{2}$; (vi) $-x+1, y+\frac{1}{2}, -z+\frac{3}{2}$; (vii) $-x+1, -y+1, -z+1$; (viii) $x, y+1, z$.

Data collection

Bruker SMART APEXII CCD area-detector diffractometer
Absorption correction: multi-scan (*SADABS*; Bruker, 2003)
$T_{\rm min}$ = 0.733, $T_{\rm max}$ = 0.820 (expected range = 0.857–0.959)
3655 measured reflections
1527 independent reflections
1355 reflections with $I > 2\sigma(I)$
$R_{\rm int}$ = 0.018

Refinement

$R[F^2 > 2\sigma(F^2)]$ = 0.027
$wR(F^2)$ = 0.065
S = 1.08
1527 reflections
146 parameters
45 restraints
All H-atom parameters refined
$\Delta\rho_{\rm max}$ = 0.33 e Å^{-3}
$\Delta\rho_{\rm min}$ = −0.34 e Å^{-3}

H-atom positions were obtained from difference Fourier maps and refined isotropically. The *SHELXL97* (Sheldrick, 2008) instruction SADI was used to restrain the O—H distances to be similar, within an effective standard uncertainty of 0.02.

Data collection: *APEX2* (Bruker, 2006); cell refinement: *SAINT* (Bruker, 2003); data reduction: *SAINT*; program(s) used to solve structure: *SHELXS97* (Sheldrick, 2008); program(s) used to refine structure: *SHELXL97* (Sheldrick, 2008); molecular graphics: *ATOMS* (Dowty, 2003); software used to prepare material for publication: *SHELXTL* (Sheldrick, 2008) and *publCIF* (Westrip, 2009).

The authors gratefully acknowledge the support of the Natural Sciences and Engineering Research Council of Canada in the form of a Discovery grant to RCP and a post-graduate scholarship to EMSL.

Supplementary data for this paper are available from the IUCr electronic archives (Reference: SQ3201). Services for accessing these data are described at the back of the journal.

References

Archibald, E. H. & Gale, W. A. (1924). *J. Am. Chem. Soc.* **46**, 1760–1771.

Baur, W. H. (1964). *Acta Cryst.* **17**, 1361–1369.

Blasdale, W. C. & Robson, H. L. (1928). *J. Am. Chem. Soc.* **50**, 35–46.

Brown, I. D. (1981). *Struct. Bond. Cryst.* **2**, 1–13.

Bruker (2003). *SADABS*, *SAINT* and *SHELXTL*. Bruker AXS Inc., Madison, Wisconsin, USA.

Bruker (2006). *APEX2*. Bruker AXS Inc., Madison, Wisconsin, USA.

Christensen, P. R. *et al.* (2004). *Science*, **306**, 1733–1739.

Dalton, J. B. (2007). *Geophys. Res. Lett.* **34**, L21205, doi:10.1029/2007GL-031497.

Dalton, J. B., Prieto-Ballesteros, O., Kargel, J. S., Jamieson, C. S., Jolivet, J. & Quinn, R. (2005). *Icarus*, **177**, 472–490.

D'Ans, J. (1933). In *Die Losungsgleichgewichte der Systeme der Salze der ozeanischen. Salzablagerungen*. Berlin: Verlagsgesellschaft für Ackerbau.

Doesburg, J. D. J. van, Vergouwen, L. & van der Plas, L. (1982). *Am. Mineral.* **67**, 1035–1038.

Dowty, E. (2003). *ATOMS*. Shape Software, Kingsport, Tennessee, USA.

Driessen, P. M. & Schoorl, R. (1973). *J. Soil Sci.* **24**, 436–442.

Eghbal, M. K., Southard, R. J. & Whittig, L. D. (1989). *Soil Sci. Soc. Am. J.* **53**, 898–903.

Fang, J. H. & Robinson, P. D. (1970). *Am. Mineral.* **55**, 378–386.

Ferraris, G. & Ivaldi, G. (1988). *Acta Cryst.* B**44**, 341–344.

Fischer, W. & Hellner, E. (1964). *Acta Cryst.* **17**, 1613.

Friedel, B. (1976). *Neues Jahrb. Mineral. Abh.* **126**, 187–198.

Gao, X., Ma, B., Yang, Y. & Su, A. (2007). *J. Mater. Eng. Perform.* **17**, 543–549.

Hawthorne, F. C. (1985). *Can. Mineral.* **23**, 669–674.

Hawthorne, F. C. & Ferguson, R. B. (1975). *Can. Mineral.* **13**, 181–187.

Kannan, K. K. & Viswamitra, M. A. (1965). *Z. Kristallogr.* **122**, 161–174.

Kargel, J. S., Kaye, J. Z., Head, J. W., Marion, G. M., Sassen, R., Crowley, J. K., Ballesteros, O. P., Grant, S. A. & Hogenboom, D. L. (2000). *Icarus*, **148**, 226–265.

Keller, L. P., McCarthy, G. J. & Richardson, J. L. (1986*a*). *Soil Sci. Soc. Am. J.* **50**, 1069–1071.

Keller, L. P., McCarthy, G. J. & Richardson, J. L. (1986*b*). *Soil Sci. Soc. Am. J.* **50**, 1363–1367.

King, P. L., Lescinsky, D. T. & Nesbitt, H. W. (2004). *Geochim. Cosmochim. Acta*, **68**, 4993–5008.

Last, W. M. (2002). *Geosci. J.* **6**, 347–369.

Last, W. M. & Ginn, F. M. (2005). *Saline Systems*, **1**, 10, doi:10.1186/1746-1448-1-10.

Leduc, E. M. S., Peterson, R. C. & Wang, R. (2009). *Am. Mineral.* **94**, 1005–1011.

Levy, H. A. & Lisensky, G. C. (1978). *Acta Cryst.* B**34**, 3502–3510.

Nord, A. G. (1973). *Acta Chem. Scand.* **27**, 814–822.

Peterson, R. C., Nelson, W., Madu, B. & Shurvell, H. F. (2007). *Am. Mineral.* **92**, 1756–1759.

Peterson, R. C. & Wang, R. (2006). *Geology*, **34**, 957–960.

Rumanova, I. M. (1958). *Dokl. Akad. Nauk SSSR*, **118**, 84–87.

Shayan, A. & Lancucki, C. J. (1984). *Soil Sci. Soc. Am. J.* **48**, 939–942.

Sheldrick, G. M. (2008). *Acta Cryst.* A**64**, 112–122.

Squyres, S. W., *et al.* (2004). *Science*, **306**, 1709–1714.

Timpson, M. E., Richardson, J. L., Keller, L. P. & McCarthy, G. J. (1986). *Soil Sci. Soc. Am. J.* **50**, 490–493.

Westrip, S. P. (2009). *publCIF*. In preparation.

Whittig, L. D., Deyo, A. E. & Tanji, K. K. (1982). *Soil Sci. Soc. Am. J.* **46**, 645–651.

Zalkin, A., Ruben, H. & Templeton, D. H. (1964). *Acta Cryst.* **17**, 235–240.

Zielinski, R. A., Otton, J. K. & Johnson, C. A. (2001). *J. Environ. Qual.* **30**, 1237–1248.